RSC Advances

PAPER

View Article Online
View Journal | View Issue



Cite this: *RSC Adv.*, 2022, **12**, 35461

# Metal–organic frameworks incorporating azobenzene-based ligands as a heterogeneous Lewis-acid catalyst for cyanosilylation of imines†

Aasim Saeed,[a] Xiao-Yu Zhang,[a] Zi-Qing Huang,[a] Xin-Yang Zhao,[a] Lei Xu,[b] Yue Zhao, *[a] Wei-Yin Sun *[a] and Jing Zhao *[a]

In this work, two novel metal–organic frameworks (MOFs) were synthesized by the reaction of azobenzene-based ligands and $Zn(NO_3)_2$/$CdCO_3$ under solvothermal conditions with the formula of $\{[Zn_2(abtc)(azpy)(H_2O)_2]\cdot 4H_2O\}_n$ (**1**) and $\{[Cd(abtc)_{0.5}(azpy)_{0.5}(H_2O)]\cdot 3H_2O\}_n$ (**2**) ($H_4$abtc = 3,3′,5,5′-azobenzene tetracarboxylic acid, azpy = 4,4′-azobipyridine). According to the single-crystal X-ray diffraction (SC-XRD) analysis, complexes **1** and **2** possessed quite similar structures except for the coordination modes of the central metal nodes attributed to the difference between the cationic radius of Zn(II) and Cd(II). The Zn(II) cations in **1** adopted a distorted seesaw coordination geometry and the coordination between Zn(II) and organic linkers gave two-dimensional (2D) coordination networks, while the Cd(II) cations in **2** could also bind with the carboxylate groups from neighboring coordination networks to form a three-dimensional (3D) coordination framework. Furthermore, complexes **1** and **2** showed high catalytic activity as heterogeneous Lewis-acid catalysts towards the cyanosilylation of imines with satisfactory reusability under mild conditions and the similar catalytic performance of **1** and **2** could be attributed to the similarity in their structures. A prudent mechanism has been proposed as well to elucidate the role of complexes **1** and **2** in the catalytic process.

Received 30th October 2022
Accepted 30th November 2022

DOI: 10.1039/d2ra06858c

rsc.li/rsc-advances



## Introduction

As a class of important intermediates, cyanohydrins have been widely used in the preparation of various high-value chemicals in chemistry and biology, such as α-amino acids, β-amino alcohols, α-hydroxy esters, and so on due to the versatile reactivity of the cyano group.[1–5] Among different synthetic approaches, the catalytic addition to unsaturated bonds (mainly C=C, C=N, and C=O bonds) by employing trimethylsilyl cyanide (TMSCN) as the cyanating reagents to give cyanohydrin trimethylsilyl ethers has been considered as one of the most efficient procedures because of the advantages of this methodology such as safety, simple operation, atom economy, no side reactions, high isolated-yields, low dissociation energy of Si–C bond and so on.[6–9] Hence, the development of catalysts for the transformation from TMSCN to cyanohydrins has drawn intensive attention and been frequently at the forefront of synthetic chemistry. In the past several decades, varieties of catalysts have been demonstrated to be efficient in this methodology but most of them are homogeneous, which leads to great difficulties in the separation and reusability of the catalysts.[10–17] In this regard, heterogeneous catalysts have caught researchers' attention because their inherent stability and ease of recovery make it simple but efficient to be separated and reused.[18–24] Therefore, it is of great significance to develop well-performed heterogeneous catalysts for the synthesis of cyanohydrins.

Metal–organic frameworks (MOFs) are a class of burgeoning inorganic–organic porous materials constructed from the coordination of multidentate organic linkers and metal cations or clusters.[25–27] Due to the ultrahigh porosity, large surface area, structural diversity and tunability, and easy modification, MOFs have stimulated great scientific interest in the past several decades and found diverse applications in various fields including gas adsorption/storage/separation, chemical sensing, drug delivery, nonlinear optics, energy storage/conversion, and catalysis, among which heterogeneous catalysis was one of the earliest proposed and demonstrated applications.[28–42] Compared with other heterogeneous catalysts, MOFs exhibited many superior characteristics derived from their structural nature. For example, the ordered architecture enables the uniform dispersion and the high density of catalytic sites to

[a]Coordination Chemistry Institute, State Key Laboratory of Coordination Chemistry, School of Chemistry and Chemical Engineering, Nanjing University, Nanjing 210023, China. E-mail: Jingzhao@nju.edu.cn; zhaoyue@nju.edu.cn; sunwy@nju.edu.cn; Tel: +86 25 89681957

[b]Jiangsu Key Lab of Data Engineering and Knowledge Service, School of Information Management, Nanjing University, Nanjing 210023, China

† Electronic supplementary information (ESI) available: PXRD, NMR, TG, IR spectra and additional figures. CCDC 2205084 and 2205086. For ESI and crystallographic data in CIF or other electronic format see DOI: https://doi.org/10.1039/d2ra06858c

improve the catalytic utility; the large enough pore could encapsulate reactants in a confined environment, which is beneficial for the sufficient contact of reactants with catalytic sites; the adjustable pore structures including pore size, hydrophilic/hydrophobic property, electron-deficient/electron-rich nature, chirality and so on endow MOFs with different affinity for various reactant molecules, which distinctly improve the catalytic selectivity.[43,44] Therefore, the rational design/synthesis and post-synthetic modification of MOFs for heterogeneous catalysis have gained particular attention recently and MOFs have been demonstrated effective as the pre, co, cooperative, or promotor catalysts in various reactions like cyanosilylation, Knoevenagel condensation, Heck and Fischer–Tropsch reactions. In terms of cyanosilylation, the most studied is the transformation from aldehydes or ketones with TMSCN but using imines as the reactants have been scarcely reported.[45–55]

In this work, 3,3′,5,5′-azobenzene tetracarboxylic acid ($H_4$abtc), 4,4′-azobipyridine (azpy), and Zn(II)/Cd(II) were employed as the organic linkers and metal nodes to elaborate novel MOFs to serve as heterogeneous catalysts for the cyanosilylation of imines. The choice of such linkers and metal nodes is attributed to the following factors: (a) $H_4$abtc has four carboxyl groups and can generate a variety of structures *via* complete or partial deprotonation; (b) the azo bond is a Lewis base group and could easily reverse its *cis* or *trans* configuration, which may enable the synthesized MOFs more structural diversity and modulate the catalytic performance; (c) the π-conjugated aromatic linkers may be beneficial to the accessibility of active sites and transport to the substrate/products in catalysis; (d) the $d^{10}$ transition metal nodes (Zn(II)/Cd(II)) could afford various Lewis acid catalytic sites.[56–62] By the reaction of $H_4$abtc, azpy, and Zn(II)/Cd(II) under solvothermal conditions, two novel MOFs with the formula of $\{[Zn_2(abtc)(azpy)(H_2O)_2]\cdot 4H_2O\}_n$ (**1**) and $\{[Cd(abtc)_{0.5}(azpy)_{0.5}(H_2O)]\cdot 3H_2O\}_n$ (**2**) were obtained. Single-crystal X-ray diffraction (SC-XRD) results revealed that these two MOFs were isostructural although complex **1** and **2** were respectively constructed from 2D and 3D coordination networks. Due to the larger radius of the metal cation, the central Cd(II) cations in **2** could form coordination bonds between the central nodes from two adjacent 2D coordination networks to form a 3D coordination framework and such a phenomenon has been scarcely reported. Furthermore, the Lewis acid nature of synthesized MOFs has been examined with their substrate scopes by heterogeneously catalyzed imine cyanosilylation reactions and experimental results showed that both complexes **1** and **2** possessed effective catalytic activity for imine cyanosilylation with favorable reusability.

# Experimental

### Materials and methods

The organic linkers $H_4$abtc and azpy were synthesized according to the previously reported procedures.[63,64] All other commercially available chemicals and solvents were of the reagent grades and used as received without further purification. The powder X-ray diffraction (PXRD) data was collected using an X-ray diffractometer equipped with Cu Kα ($\lambda = 1.54184$ Å; 20 mA, 40 kV) radiation in the 2-theta range of 5–50° on a Bruker D8 Advance X-ray diffractometer. Thermogravimetric analysis (TGA) was conducted on a Mettler-Toledo (TGA/DSC1) thermal analyzer with a heating rate of 10 °C $min^{-1}$ under an $N_2$ atmosphere in the temperature range of 25–800 °C. Fourier transform infrared-attenuated total internal reflectance (FTIR-ATR) spectra were measured on a Bruker Tensor II spectrophotometer equipped with a diamond ATR module using the mid-IR region (4000–400 $cm^{-1}$). PerkinElmer's 240C elemental analyzer was used to carry out the elemental analysis (EA) of C, H, and N. The reactions were monitored with thin-layer chromatography (TLC) on silica gel plates (HSGF254). $^1H$ and $^{13}C$ NMR spectra were recorded at room temperature on Bruker-DRX 400 MHz instrument and the chemical shifts were reported in parts per million (ppm) with tetramethyl silane or the residual solvent peak as an internal reference. High-resolution mass (HRMS) spectra were performed on a Thermo Fischer QExactive quadrupole-Orbitrap mass spectrometer.

**Synthesis of $\{[Zn_2(abtc)(azpy)(H_2O)_2]\cdot 4H_2O\}_n$ (1).** $H_4$abtc (35.8 mg, 0.1 mmol), $Zn(NO_3)_2\cdot 6H_2O$ (59.5 mg, 0.2 mmol) and azpy (36.4 mg, 0.2 mmol) were dissolved in deionized water (3 mL) and *N*,*N*-dimethylacetamide (DMA, 5 mL), followed by the addition of concentrated $HNO_3$ (68%, 40 μL) and stirred well for 30 minutes at room temperature. Then, the resultant reaction mixture was sealed in a 10 mL Pyrex tube and heated at 85 °C for 72 h. After cooling down to ambient temperature, brown crystals of **1** were isolated by filtration and washed several times with $H_2O$. Yield: 85% (based on $H_4$abtc). Anal. Calc. for $C_{26}H_{26}N_6O_{14}Zn_2$: C 40.18; H 3.37; N 10.81%. Found: C 40.57; H 3.27; N 11.08%. FTIR-ATR ($cm^{-1}$, Fig. S3†): 3311 (m), 1614 (s), 1430 (m), 1343 (s), 1220 (m), 1104 (w), 850 (w), 768 (m), 727 (m), 565 (w), 522 (w).

**Synthesis of $\{[Cd(abtc)_{0.5}(azpy)_{0.5}(H_2O)]\cdot 3H_2O\}_n$ (2).** The preparation of **2** was similar to that of **1** except that $CdCO_3$ (34.4 mg, 0.2 mmol) was used instead of $Zn(NO_3)_2\cdot 6H_2O$ and the reaction time was extended to 90 h. After filtration and washing with $H_2O$, orange crystals of **2** could be obtained in 89% yield (based on $H_4$abtc). Anal. Calc. for $C_{13}H_{15}CdN_3O_8$: C 34.42; H 3.33; N 9.26%. Found: C 35.35; H 3.12; N 9.58%. FTIR-ATR ($cm^{-1}$, Fig. S3†): 3414 (m), 1602 (s), 1561 (s), 1373 (s), 1250 (m), 1107 (w), 849 (w), 813 (m), 733 (m), 567 (w), 499 (w).

**The heterogeneous catalytic cyanosilylation of imines.** The catalyst **1** and **2** (0.1 mmol), aldimine (0.5 mmol), and trimethylsilyl cyanide (0.75 mmol, TMSCN) were placed into a 25 mL three-neck round bottom flask and the whole reaction mixture was stirred at ambient temperature for the given time under a $N_2$ atmosphere. The reaction was monitored by thin-layer chromatography (TLC) using ethyl acetate/*n*-hexane (1 : 9) as the developing solvent. After the reaction was completed, the reaction mixture was filtered carefully to separate the catalyst as residue, and the filtrate containing the final product was then evaporated under a vacuum, which then was neutralized by adding 5 mL of 1% $NaHCO_3$ solution and extracted with ethyl acetate. The ethyl acetate layer was dried over anhydrous $Na_2SO_4$, and the crude product was obtained by evaporating the ethyl acetate under vacuum and then purified by using column chromatography (silica gel, 100–200 mesh) with ethyl acetate/*n*-

hexane (1 : 12 v/v) as the eluent. In addition, the separated catalyst residue was washed with DCM multiple times, air-dried for about four hours, and then reused for the following run-up to 5 cycles.

**The cycle experiments.** After the catalytic reactions, the solid catalysts **1** and **2** were collected by centrifugation, washed with ethanol several times and then dried in an oven at 60 °C. Afterward, the recovered catalysts **1** and **2** were directly introduced into the reaction system again to catalyze the reaction of benzylideneaniline with TMSCN under the same conditions.

### X-ray crystallography

Suitable single crystals of **1** and **2** were mounted on a cryoloop using Paratone N oil, and then the crystallographic data collections were carried out on a Bruker D8 Venture diffractometer equipped with graphite-monochromated Ga Kα radiation ($\lambda$ = 1.34139 Å) and a Bruker D8 Venture Photon 100 diffractometer equipped with graphite-monochromated Mo Kα radiation ($\lambda$ = 0.71073 Å) using the $\varphi$–$\omega$ scan technique, respectively. SAINT program was used to integrate diffraction data and the intensity corrections for Lorentz and polarization effects.[65] Semi-empirical absorption corrections were applied using SADABS program.[66] The structures were solved by direct methods with SHELXT-2014, expanded by subsequent Fourier-difference synthesis, and all the non-hydrogen atoms were refined anisotropically on $F^2$ using the full-matrix least-squares technique using the SHELXL-2018 crystallographic software package.[67] Hydrogen atoms except those of water molecules were introduced at the calculated positions and refined isotopically using a riding model. The hydrogen atoms of water molecules were located based on the Fourier difference maps. The free solvent molecules in the unit cell of **2** were taken into account using SQUEEZE option of the PLATON program.[68] The final formula of **2** was calculated based on volume/count electron analysis, TGA, and EA, and the results were attached to the CIF file. Structural refinement details and crystallographic data for **1** and **2** are given in Table 1 and the selected bond lengths and angles are given in Table S1.†

Table 1 Crystal data and structure refinement parameters of **1** and **2**[ab]

| | **1** | **2** |
|---|---|---|
| Empirical formula | $C_{26}H_{26}N_6O_{14}Zn_2$ | $C_{13}H_9CdN_3O_5$ |
| Formula mass | 777.2 | 399.64 |
| Crystal system | Triclinic | Triclinic |
| Space group | $P\bar{1}$ | $P\bar{1}$ |
| $a$ (Å) | 7.8726 (3) | 7.5893 (8) |
| $b$ (Å) | 9.1910 (3) | 9.8529 (11) |
| $c$ (Å) | 11.7294 (4) | 12.2846 (13) |
| $\alpha$ (°) | 96.2350 (10) | 100.780 (4) |
| $\beta$ (°) | 104.8540 (10) | 99.296 (3) |
| $\gamma$ (°) | 112.3330 (10) | 109.467 (4) |
| $V$ (Å$^3$) | 738.39 (5) | 825.58 (16) |
| $Z$ | 1 | 2 |
| $T$/K | 193 (2) | 296 (2) |
| $\rho_{calcd}$ (g cm$^{-3}$) | 1.748 | 1.608 |
| $\mu$ (mm$^{-1}$) | 1.794 | 1.346 |
| $\lambda$ (Å) | 1.34139 (Ga Kα) | 0.71073 (Mo Kα) |
| $\theta_{min}$ (°) | 4.650 | 2.270 |
| $\theta_{max}$ (°) | 53.880 | 27.478 |
| Reflection collected | 7625 | 7402 |
| Unique reflections | 2661 | 3745 |
| $R_{int}$ | 0.0331 | 0.0310 |
| $R$ indexes [$I > 2\sigma(I)$] | $R_1$ = 0.0377, w$R_2$ = 0.1033 | $R_1$ = 0.0280, w$R_2$ = 0.0697 |
| $R$ indexes (all data) | $R_1$ = 0.0401, w$R_2$ = 0.1053 | $R_1$ = 0.0316, w$R_2$ = 0.0716 |
| $F$(000) | 396 | 392 |
| GOF on $F^2$ | 1.028 | 1.047 |

[a] $R_1 = \sum||F_o| - |F_c||/\sum|F_o|$. [b] $wR_2 = [\sum w(F_o^2 - F_c^2)^2/\sum w(F_o^2)^2]^{1/2}$, where $w = 1/[\sigma^2(F_o)^2 + (aP)^2 + bP]$.

## Results and discussion

### Crystal structure description

**Crystal structure of 1.** Crystallographic analysis revealed that complex **1** was crystallized in the triclinic $P\bar{1}$ space group and the asymmetric unit was comprised of a crystallographically independent Zn(II) cation, one-half completely deprotonated carboxylate linker abtc$^{4-}$, half an azpy linker, one coordinated and two lattice $H_2O$ molecules. As shown in Fig. 1a, atom Zn1 exhibited a seesaw geometry ($\tau_4$ = 0.78),[69] furnished by two carboxylate oxygen (O1, O3#1) atoms from two discrete abtc$^{4-}$ linkers, one nitrogen atom (N2) belonging to azpy linker, and one coordinated $H_2O$ molecule (O5). The Zn–N bond length was 2.024(2) Å, and the bond lengths observed between Zn–O were in the range of 1.9309(18)–2.049(2) Å (Table S1†). Additionally, the coordination bond angles surrounding the Zn(II) nodes vary in the range of 93.75(8)–128.77(9)° (Table S1†). The complete deprotonation of the carboxylic groups of the organic linker $H_4$abtc was also demonstrated by the absence of the infrared absorption characteristic peaks of –COOH around 1700 cm$^{-1}$ in FTIR-ATR spectra (Fig. S3†). The Zn(II) nodes were bridged by the carboxylate groups of abtc$^{4-}$ linkers to form 1-dimensional (1D) ladder-like coordination chains (Fig. 1b), which were further linked by azpy linker to generate 2-dimensional (2D) coordination networks with two kinds of windows with the Zn···

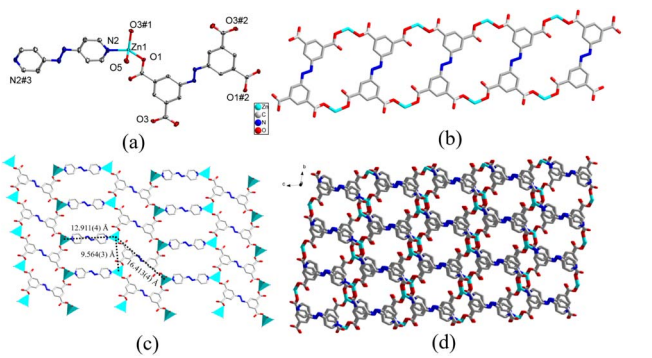


Fig. 1 (a) Coordination environment of Zn(II) atoms in **1** with the ellipsoid drawn at the 30% probability level. Symmetry code: #1 $-x + 1$, $-y + 1$, $z$; #2 $-x + 1$, $-y + 1$, $-z + 2$; #3 $-x$, $-y - 1$, $-z$. (b) 1D coordination ladders constructed from Zn(II) and abtc$^{4-}$, (c) 2D coordination networks, (d) 3D supramolecular framework along $a$-axis in **1**. Hydrogen atoms and free $H_2O$ molecules are omitted for clarity.

Zn distances of 9.564(3) × 12.911(3) Å and 9.564(3) × 16.413(4) Å (Fig. 1c). Furthermore, these 2D networks could be stacked in a staggered mode to form a 3-dimensional (3D) supramolecular framework (Fig. 1d and S1a and S1b†) with 1D channels along *a*-axis through π···π interactions between the benzene ring of $abtc^{4-}$ and the pyridine ring of azpy and the hydrogen bonds among the lattice waters, coordinated waters and organic linkers from the 2D networks (Fig. S1c†). According to the result of PLATON, the porosity of complex **1** was calculated to be 15.7%. In addition, the unusual bond length between the metal centre and carboxylate oxygen (Zn1–O1#4 = 2.7810(1), Fig. S1d†) from adjacent layer suggested a non-negligible weak interaction. Hence, the geometry around the Zn(II) centre in **1** may also be regarded as a distorted trigonal bipyramid and bridged by the carboxylate oxygen atom to form binuclear Zn(II) centre. Therefore, taking the weak Zn–O interaction into consideration, each binuclear Zn(II) cluster was bound to six organic linkers and thus could be regarded as a six-connected node, while the organic linker $abtc^{4-}$ and azpy could be similarly treated as four-connected and two-connected nodes respectively from the point view of topology. Hence, the structure of complex **1** could be simplified as a (2,4,6)-connected framework with the topological symbol of $\{4^4\cdot6^{10}\cdot8\}\ \{4^4\cdot6^2\}$ (Fig. S1e†) using the TOPOS program,[70] which was also reported in some other MOFs.[71]

**Crystal structure of 2.** The SC-XRD measurement results showed that complex **2** was also crystallized in the triclinic system with the $P\bar{1}$ space group and each asymmetric unit of **2** was comprised of a crystallographically independent Cd(II) node, half one $abtc^{4-}$ organic anion, half one azpy molecule, and one coordinated $H_2O$ molecule. Structural analysis revealed that the structure of complex **2** was almost identical to that of **1** except for the coordination modes of central metal cations. Compared to complex **1**, due to the large ionic radius of Cd(II) than Zn(II) cation, the central Cd(II) cations could also coordinate with the carboxylate groups from the adjacent network to form binuclear clusters (Fig. 2b) and thus the coordination geometry of central Cd1 atoms was a six-coordinated octahedron surrounded by one nitrogen atom (N1) from the pyridine ring of azpy ligand, four carboxylate oxygen atoms (O2, O3, O4#1, O5#2) from two different $abtc^{4-}$ linkers and one coordinated water (O1) molecule (Fig. 2a). The Cd–N bond length was 2.303(2) Å, and the Cd–O bond lengths were observed in a typical range of 2.269(2)–2.596(2) Å (Table S1†). The O–Cd–O and O–Cd–N bond angles varied in the range of 53.04(7)–171.15(9)° and 84.98(9)–138.80(9)°, respectively (Table S1†). The coordination between Cd(II) cations and organic ligands $abtc^{4-}$ led to the formation of 2D coordination networks possessing the windows with the Cd1–Cd1 distances of 10.239(1) × 12.284(6) Å (Fig. 2c and S2a†), which were bridged by linker azpy to generate 3D coordination frameworks with 1D channels along *a*-axis through the connection between Cd(II) cations and pyridine of azpy (Fig. 2d). The porosity of complex **2** could be calculated to be 23.6% using PLATON software. Furthermore, according to the topological analysis, the structure of complex **2** had the same topological structure as that of **1** with the topological symbol of $\{4^4\cdot6^{10}\cdot8\}\ \{4^4\cdot6^2\}$ (Fig. S2b†).

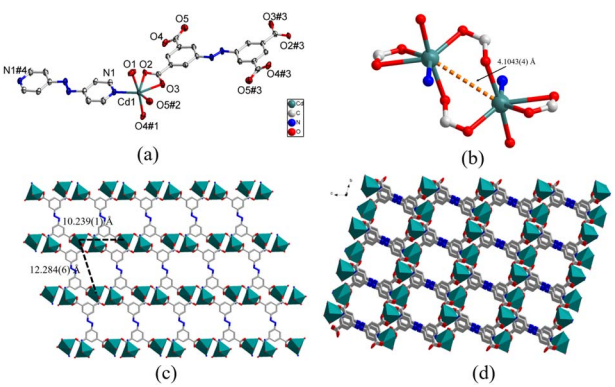


Fig. 2 (a) Coordination environment of Cd(II) atoms in **2** with the ellipsoid drawn at the 30% probability level. Symmetry code: #1 −*x*, −*y* + 1, −*z* + 1; #2 *x* + 1, *y* + 1, *z*; #3 −*x*, −*y* + 1, −*z* + 2; #4 −*x* + 1, −*y* + 1, −*z*. (b) The structure of binuclear $Cd_2$ node in **2**. (c) 2D coordination networks in **2** constructed from Cd(II) cations and ligand $abtc^{4-}$. (d) 3D coordination framework of **2** along the *a*-axis. Hydrogen atoms were omitted for clarity.

## Chemical and thermal stability

PXRD was employed to check the phase purities and investigate the chemical stability of synthesized complexes **1** and **2**. As shown in Fig. S4,† the PXRD patterns of the as-synthesized samples of **1** and **2** were almost identical to the simulated ones obtained from the single-crystal data, demonstrating the phase purities and crystallinity of synthesized complexes **1** and **2**. Furthermore, the PXRD patterns of complexes **1** and **2** remained unchanged after exposing to air for one month, immersed in different organic solvents for one week including dichloromethane (DCM), ether ($Et_2O$), tetrahydrofuran (THF), acetone, acetonitrile (MeCN), methanol (MeOH), ethanol (EtOH), *n*-hexane, ethyl acetate (EA), DMA, *N*,*N*-dimethylformamide (DMF) and dimethyl sulfoxide (DMSO), and soaking in water within the pH range from 1 to 13 and boiling water for at least one day (Fig. S5 and S6†), which demonstrated the ultrahigh chemical stability of complexes **1** and **2**. Furthermore, the thermal stability of complexes **1** and **2** was also investigated by thermogravimetric (TG) measurements. As shown in Fig. S7a,† complex **1** exhibited a weight loss of 9.6% in the range of 25–110 °C and then 4.6% before 170 °C, corresponding to the release of the lattice water molecules (calcd. 9.3%) and coordinated water molecules (calcd. 4.6%), respectively. Further weight loss revealed that its framework could retain up to 310 °C. As for complex **2** shown in Fig. S7b,† the initial weight loss in the temperature range of 25–135 °C was about 11.1%, which could be attributed to the removal of lattice water molecules (calcd. 11.9%). The second weight loss before 220 °C was about 3.0%, corresponding to the release of the coordinated water (calcd. 4.0%). And then the structure of complex **2** started to decompose until 315 °C. These results demonstrated that complexes **1** and **2** not only possessed outstanding chemical stability but also had fairly high thermal stability.

### Gas adsorption behaviors

Prior to gas adsorption, as-synthesized porous frameworks **1** and **2** were activated by heating at 170 and 180 °C under dynamic vacuum overnight, respectively. The TG curves and the PXRD patterns of the activated **1** and **2** indicated the removal of solvents and the retainment of their framework structure (Fig. S7 and S8†). The adsorption isotherms of the activated samples of **1** and **2** for $N_2$ were monitored at 77 K. The results revealed that they both displayed the typical reversible type-II $N_2$ adsorption isotherm and the maximum $N_2$ sorption capacity for 1 and 2 was both 0.5 mmol $g^{-1}$ under 0.99 bar. The Brunauer–Emmett–Teller (BET) surface area based on the $N_2$ sorption data was calculated to be 6.5 $m^2$ $g^{-1}$ and 15.2 $m^2$ $g^{-1}$ for **1** and **2**, respectively (Fig. S9a and b†). Furthermore, the $CO_2$ adsorption isotherms were collected at 273 K and 298 K for the guest-free frameworks **1** and **2** as well. The obtained adsorption isotherms exhibited the maximum $CO_2$ sorption capacity was 0.15, 1.52 mmol $g^{-1}$ at 273 K and 0.040, 0.77 mmol $g^{-1}$ at 298 K for **1** and **2**, respectively under 800 mmHg (Fig. S9c and d†). This indicate that the pores in the structures are very small, and the catalytic reactions occur on the surface of the catalysts.

### Catalytic activity for the cyanosilylation of imines

In consideration of the presence of coordinated water molecules enabling the central metal nodes as the potential vacant metal coordination metal sites, complexes **1** and **2** may be used as a Lewis acid heterogeneous catalyst and their catalytic performance for the cyanosilylation of imines was investigated. First of all, benzylideneaniline was chosen as the model substrate to check the catalytic activity of complexes **1** and **2** for the cyanosilylation with TMSCN and optimize the reaction conditions. As shown in Table 2, it could be clearly found that the yields of the cyanosilylation reaction improved distinctly with time and reach up to 95% for **1** and 98% for **2** in 4 h at room temperature with DCM as the solvent (entry 1–4 and 8–11). More, the influence of solvent and temperature were also checked and it could be found that the yields of the cyanosilylation reaction in the ice-water bath (0 °C) and in THF or ethyl ether as solvent were all obviously lower than those at room temperature in DCM (entry 5–7 and 12–14). Therefore, the catalytic cyanosilylation reactions were carried out at room temperature in DCM. In addition, it could be also found that the reaction yields were much lower without any catalyst or with the metal salts $Zn(NO_3)_2/CdCO_3$ or the organic ligands $H_4$abtc and azpy as the catalyst (entry 15–19), which indicated the catalytic

Table 2 Optimized conditions for the imine cyanosilylation with complexes **1** and **2** as catalysts[a]

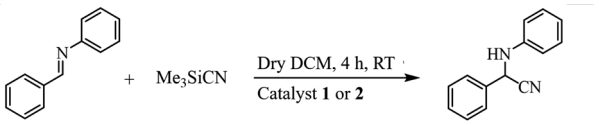


| Catalyst | Solvent | Temperature (°C) | Time (h) | Yield (%) | TON |
|---|---|---|---|---|---|
| **1** | DCM | RT | 4 | 95 | 4.75 |
| | DCM | RT | 3 | 75 | 3.75 |
| | DCM | RT | 2 | 59 | 2.95 |
| | DCM | RT | 1 | 43 | 2.15 |
| | DCM | 0 | 4 | 61 | 3.05 |
| | THF | RT | 4 | 63 | 3.15 |
| | $(C_2H_5)_2O$ | RT | 4 | 69 | 3.45 |
| **2** | DCM | RT | 4 | 98 | 4.90 |
| | DCM | RT | 3 | 79 | 3.95 |
| | DCM | RT | 2 | 62 | 3.10 |
| | DCM | RT | 1 | 49 | 2.45 |
| | DCM | 0 | 4 | 66 | 3.30 |
| | THF | RT | 4 | 71 | 3.55 |
| | $(C_2H_5)_2O$ | RT | 4 | 93 | 4.65 |
| $Zn(NO_3)_2 \cdot 6H_2O$ | DCM | RT | 4 | 23 | 1.15 |
| $CdCO_3$ | DCM | RT | 4 | 13 | 0.65 |
| $H_4$abtc | DCM | RT | 4 | 7 | 0.35 |
| azpy | DCM | RT | 4 | 6 | 0.30 |
| Blank | DCM | RT | 4 | 6 | 0.30 |

[a] Reaction conditions: *N*-benzylideneaniline (0.5 mmol), $Me_3SiCN$ (0.75 mmol), dry DCM (4 mL), catalysts **1** and **2**, linkers $H_4$abtc, azpy (0.1 mmol), blank reaction, 4 h.

Table 3 Substrate scope for the imine cyanosilylation heterogeneously catalyzed by **1** and **2**

| Entry no. | Substrates | Products | Yield[a] (%) **1** | Yield[a] (%) **2** |
|---|---|---|---|---|
| 1 | 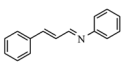 | 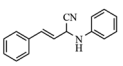 | 89 | 91 |
| 2 | 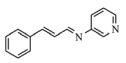 | 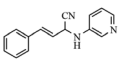 | 87 | 90 |
| 3 | 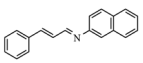 | 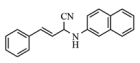 | 86 | 88 |
| 4 | 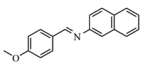 | 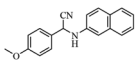 | 86 | 88 |
| 5 | 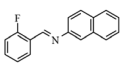 | 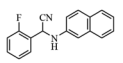 | 86 | 87 |
| 6 | 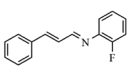 | 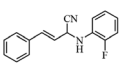 | 87 | 89 |
| 7 | 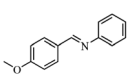 | 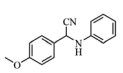 | 91 | 94 |
| 8 | 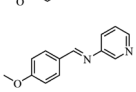 | 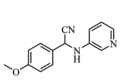 | 86 | 87 |
| 9 | 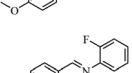 | 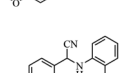 | 88 | 90 |
| 10 | 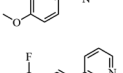 | 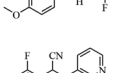 | 87 | 89 |
| 11 | 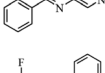 | 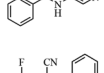 | 89 | 92 |

[a] All the reported yields in the table are average isolated yields.

activity of complexes **1** and **2** for the cyanosilylation of imines with TMSCN and the significance of the formation of MOFs for the catalytic reactions.

Next, the catalytic versatility of complexes **1** and **2** for the cyanosilylation reaction of other aromatic imines were explored. As shown in Table 3, varieties of aromatic imines bearing different electron-withdrawing or electron-donating groups were chosen to react with TMSCN under similar conditions using complexes **1** and **2** as the catalysts, and the results clearly revealed that all of these compounds could be successfully transformed into the corresponding nitrile compounds with the yields higher than 85%. Meanwhile, it could be also found that the yields with these compounds as the substrate were all lower than those of benzylideneaniline and electron-withdrawing groups afforded higher yields than electron-donating groups on the reactions because they could help the reaction activate more electrophilic sites on the reactants. In addition, it could be observed that the catalytic performance of complex **1** and **2** towards the cyanosilylation of all the selected substrates was nearly the same and the reason may be attributed to the similarity in their structure.

Furthermore, filtration tests were also conducted to examine whether complexes **1** and **2** worked in a heterogeneous manner to promote the cyanosilylation reaction of imines. Taking the cyanosilylation of benzylideneaniline as the model reaction, the reaction mixture was filtrated to remove the solid catalyst after the reaction time of 2 h, and then it could be observed that the conversion of benzylideneaniline almost remained unchanged and significantly lower than the reactions with catalyst, which obviously verified the heterogeneous nature of catalyst **1** and **2** (Fig. 4). Finally, recycling experiments were carried out to explore the reusability of complexes **1** and **2** as the catalysts for the cyanosilylation of imines. PXRD measurements revealed that PXRD patterns of **1** and **2** after catalytic reactions matched well with those simulated ones obtained from the SC-XRD data, which suggested their structural stability in the process of catalytic reactions and thus afforded the possibility of reusability (Fig. S10†). After the catalytic reactions, the solid catalysts **1** and **2** were collected by centrifugation, washed with ethanol several times and then dried in an oven at 60 °C. Afterward, the recovered catalysts **1** and **2** were directly

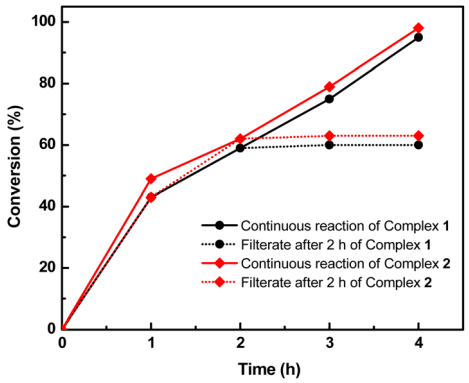


Fig. 4 The filtration test of the cyanosilylation of benzylideneaniline catalyzed by complexes **1** and **2** determined by NMR.

introduced into the reaction system again to catalyze the reaction of benzylideneaniline with TMSCN and the yields showed no significant decay even after five cycles (Fig. 3), indicating the satisfactory reusability of complexes **1** and **2** as the catalysts for the cyanosilylation of imines.

Based on the experimental results and the comparison with previously reported results (Table S3†), a possible reaction mechanism was proposed to illustrate the catalytic process of complexes **1** and **2** for the cyanosilylation of imines. In consideration of the existence of lone pairs at the nitrogen atoms in imines and Lewis acid metal nodes in complexes **1** and **2**, a weak connection may be formed between the nitrogen atoms of imines and metal nodes. Meanwhile, the coordinated oxygen atoms could act as an electron-rich nucleophilic moiety to facilitate the electron transfer to the trimethylsilyl groups of TMSCN, which resulted in the formation of weakly coordinated Si–O bonds. Meanwhile, the coordinated water molecules also may contribute to the silicon intermediate production that included the weaker C–Si link with the Lewis acid sites. As a final step, electrons from the nucleophilic –CN group were

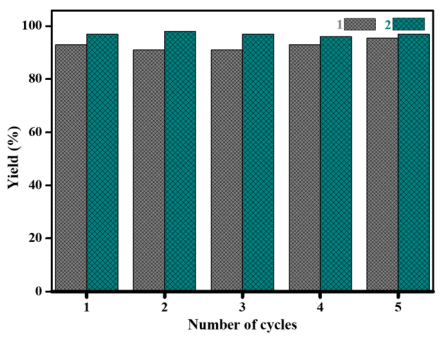


Fig. 3 Recyclability of complexes **1** and **2** as the catalysts during cyanosilylation reaction of benzylideneaniline up to 5 consecutive cycles.

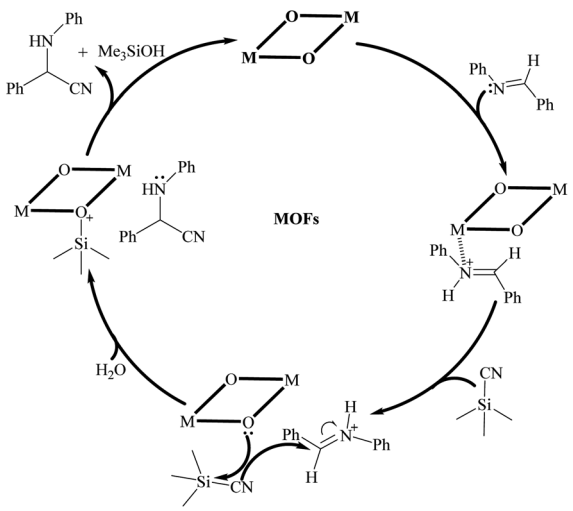


Scheme 1 Lewis acid catalyzed imine cyanosilylation proposed mechanism for catalyst **1** and **2**.

transferred to carbon to create the cyanosilylated species. The whole catalytic process was depicted in Scheme 1. Such an arrangement allows for more effective use of heterogeneous catalysts in subsequent cycles. Furthermore, the results of gas adsorption experiments and the catalytic performance for different substrates also revealed that the catalytic reaction occurred on the surface of catalyst but not in the pores of the synthesized MOFs.

## Conclusions

In conclusion, two novel MOFs **1** and **2** have been synthesized by the solvothermal reaction of azobenzene-containing ligands $H_4$abtc and azpy with $Zn(NO_3)_2$/$CdCO_3$. Although the SC-XRD analysis showed that complexes **1** and **2** were isostructural, the difference in the cationic radius of Zn(II) and Cd(II) resulted in distinctly different coordination geometry, which led to the formation of 2D coordination networks for **1** but 3D coordination frameworks for **2**. Complexes **1** and **2** both exhibited ultrahigh chemical and fairly high thermal stability. In addition, the catalytic experiments manifested that both complexes **1** and **2** had high catalytic activity as heterogeneous Lewis-acid catalysts for the imine cyanosilylation reactions under mild conditions with well-performed reusability. We believe this work will stimulate further efforts to develop new frameworks with multidentate ligands to explore new functional applications for various chemical transformations.

## Conflicts of interest

There are no conflicts of interest to declare.

## Acknowledgements

We acknowledge the National Natural Science Foundation of China (grant nos. 21401099, 21671099 and 91753121) and the Shenzhen Basic Research Program (JCYJ20180508182240106).

## Notes and references

1 J. J. Du, X. Zhang, X. P. Zhou and D. Li, *Inorg. Chem. Front.*, 2018, **5**, 2772–2776.
2 W. Wang, M. Luo, J. Li, S. A. Pullarkat and M. Ma, *Chem. Commun.*, 2018, **54**, 3042–3044.
3 F. Garnes-portolés, M. Á. Rivero-crespo and A. Leyva-pérez, *J. Catal.*, 2020, **392**, 21–28.
4 J. M. Brunel and I. P. Holmes, *Angew. Chem., Int. Ed.*, 2004, **43**, 2752–2778.
5 D. H. Ryu and E. J. Corey, *J. Am. Chem. Soc.*, 2004, **126**, 8106–8107.
6 M. North, D. L. Usanov and C. Young, *Chem. Rev.*, 2008, **108**, 5146–5226.
7 Z. Zhang, J. Chen, Z. Bao, G. Chang, H. Xing and Q. Ren, *RSC Adv.*, 2015, **5**, 79355–79360.
8 G. K. Surya Prakash, H. Vaghoo, C. Panja, V. Surampudi, R. Kultyshev, T. Mathew and G. A. Olah, *Proc. Natl. Acad. Sci. U. S. A.*, 2007, **104**, 3026–3030.
9 J. M. Pérez, S. Rojas, A. García-García, H. Montes-Andrés, C. R. Martínez, M. S. Romero-Cano, D. Choquesillo-Lazarte, V. K. Abdelkader-Fernández, M. Pérez-Mendoza, J. Cepeda, A. Rodríguez-Diéguez and I. Fernández, *Inorg. Chem.*, 2022, **61**, 1377–1384.
10 G. Cainelli, D. Giacomini, A. Treré and P. Galletti, *Tetrahedron: Asymmetry*, 1995, **6**, 1593–1600.
11 L. Mei, S. Jie and J. Ying, *Res. Chem. Intermed.*, 2010, **36**, 227–236.
12 S. Pahar, G. Kundu and S. S. Sen, *ACS Omega*, 2020, **5**, 25477–25484.
13 S. J. Zuend and E. N. Jacobsen, *J. Am. Chem. Soc.*, 2007, **129**, 15872–15883.
14 S. Rawat, M. Bhandari, B. Prashanth and S. Singh, *ChemCatChem*, 2020, **12**, 2407–2411.
15 H. Deka, N. Fridman and M. S. Eisen, *Inorg. Chem.*, 2022, **61**, 3598–3606.
16 D. E. Fuerst and E. N. Jacobsen, *J. Am. Chem. Soc.*, 2005, **127**, 8964–8965.
17 Z. Z. Weng, J. Xie, K. X. Huang, J. P. Li, L. S. Long, X. J. Kong and L. S. Zheng, *Inorg. Chem.*, 2022, **61**, 4121–4129.
18 M. Malmir and M. M. Heravi, *Sci. Rep.*, 2022, **12**, 11573.
19 C. Baleizão, B. Gigante, H. Garcia and A. Corma, *J. Catal.*, 2004, **221**, 77–84.
20 S. Zhao, Y. Chen and Y. F. Song, *Appl. Catal., A*, 2014, **475**, 140–146.
21 K. Iwanami, J. C. Choi, B. Lu, T. Sakakura and H. Yasuda, *Chem. Commun.*, 2008, **2**, 1002–1004.
22 S. Zhang, B. Zhang, H. Liang, Y. Liu, Y. Qiao and Y. Qin, *Angew. Chem., Int. Ed.*, 2018, **57**, 1091–1095.
23 K. Yamaguchi, T. Imago, Y. Ogasawara, J. Kasai, M. Kotani and N. Mizuno, *Adv. Synth. Catal.*, 2006, **348**, 1516–1520.
24 Y. X. Wang, H. M. Wang, P. Meng, D. X. Song, J. J. Hou and X. M. Zhang, *Dalton Trans.*, 2021, **50**, 1740–1745.
25 N. W. Ockwig, O. Delgado-Friedrichs, M. O'Keeffe and O. M. Yaghi, *Acc. Chem. Res.*, 2005, **38**, 176–182.
26 S. Natarajan and P. Mahata, *Chem. Soc. Rev.*, 2009, **38**, 2304–2318.
27 O. K. Farha and J. T. Hupp, *Acc. Chem. Res.*, 2010, **43**, 1166–1175.
28 J. R. Li, R. J. Kuppler and H. C. Zhou, *Chem. Soc. Rev.*, 2009, **38**, 1477–1504.
29 M. D. Allendorf, C. A. Bauer, R. K. Bhakta and R. J. T. Houk, *Chem. Soc. Rev.*, 2009, **38**, 1330–1352.
30 J. Lee, O. K. Farha, J. Roberts, K. A. Scheidt, S. T. Nguyen and J. T. Hupp, *Chem. Soc. Rev.*, 2009, **38**, 1450–1459.
31 Z. Hu, B. J. Deibert and J. Li, *Chem. Soc. Rev.*, 2014, **43**, 5815–5840.
32 V. Stavila, A. A. Talin and M. D. Allendorf, *Chem. Soc. Rev.*, 2014, **43**, 5994–6010.
33 W. Xia, A. Mahmood, R. Zou and Q. Xu, *Energy Environ. Sci.*, 2015, **8**, 1837–1866.
34 L. Sun, M. G. Campbell and M. Dincă, *Angew. Chem., Int. Ed.*, 2016, **55**, 3566–3579.
35 L. Wang, Y. Han, X. Feng, J. Zhou, P. Qi and B. Wang, *Coord. Chem. Rev.*, 2016, **307**, 361–381.

36 R. Medishetty, J. K. Zaręba, D. Mayer, M. Samoć and R. A. Fischer, *Chem. Soc. Rev.*, 2017, **46**, 4976–5004.
37 M. X. Wu and Y. W. Yang, *Adv. Mater.*, 2017, **29**, 1606134.
38 A. Gheorghe, M. A. Tepaske and S. Tanase, *Inorg. Chem. Front.*, 2018, **5**, 1512–1523.
39 P. C. Rao and S. Mandal, *Chem.–Asian J.*, 2019, **14**, 4087–4102.
40 M. Sadakiyo, *Nanoscale*, 2022, **14**, 3398–3406.
41 N. R. Habib, E. Asedegbega-Nieto, A. M. Taddesse and I. Diaz, *Dalton Trans.*, 2021, **50**, 10340–10353.
42 M. Liu, J. Wu and H. Hou, *Chem.–Eur. J.*, 2019, **25**, 2935–2948.
43 A. Yadav and P. Kanoo, *Chem.–Asian J.*, 2019, **14**, 3531–3551.
44 C. De Wu and M. Zhao, *Adv. Mater.*, 2017, **29**, 1605446.
45 J. Z. Gu, S. M. Wan, W. Dou, M. V. Kirillova and A. M. Kirillov, *Inorg. Chem. Front.*, 2021, **8**, 1229–1242.
46 C. Zhu, Q. Xia, X. Chen, Y. Liu, X. Du and Y. Cui, *ACS Catal.*, 2016, **6**, 7590–7596.
47 D. Dang, P. Wu, C. He, Z. Xie and C. Duan, *J. Am. Chem. Soc.*, 2010, **132**, 14321–14323.
48 M. Gustafsson, A. Bartoszewicz, B. Martiín-Matute, J. Sun, J. Grins, T. Zhao, Z. Li, G. Zhu and X. Zou, *Chem. Mater.*, 2010, **22**, 3316–3322.
49 F. Z. Jin, C. C. Zhao, H. C. Ma, G. J. Chen and Y. Bin Dong, *Inorg. Chem.*, 2019, **58**, 9253–9259.
50 W. Jiang, J. Yang, Y. Y. Liu, S. Y. Song and J. F. Ma, *Inorg. Chem.*, 2017, **56**, 3036–3043.
51 L. Hu, G. X. Hao, H. D. Luo, C. X. Ke, G. Shi, J. Lin, X. M. Lin, U. Y. Qazi and Y. P. Cai, *Cryst. Growth Des.*, 2018, **18**, 2883–2889.
52 N. Kumar, T. Rom, V. Singh and A. K. Paul, *Cryst. Growth Des.*, 2020, **20**, 5277–5288.
53 N. Kumar and A. K. Paul, *Inorg. Chem.*, 2020, **59**, 1284–1294.
54 D. Sarma, K. V. Ramanujachary, N. Stock and S. Natarajan, *Cryst. Growth Des.*, 2011, **11**, 1357–1369.
55 J. Chai, P. Zhang, J. Xu, H. Qi, J. Sun, S. Jing, X. Chen, Y. Fan and L. Wang, *Inorg. Chim. Acta*, 2018, **479**, 165–171.
56 Y. P. Li, L. J. Zhang and W. J. Ji, *J. Mol. Struct.*, 2017, **1133**, 607–614.
57 B. Ma, Y. Fan, L. Wang, J. Xu and J. Zhao, *Inorg. Chim. Acta*, 2018, **480**, 166–172.
58 W. Liu, L. Ye, X. Liu, L. Yuan, J. Jiang and C. Yan, *CrystEngComm*, 2008, **10**, 1395–1403.
59 B. Parmar, P. Patel, V. Murali, Y. Rachuri, R. I. Kureshy, N. U. H. Khan and E. Suresh, *Inorg. Chem. Front.*, 2018, **5**, 2630–2640.
60 R. A. Agarwal and D. De, *Polyhedron*, 2020, **185**, 114584.
61 H. Chen, L. Fan and X. Zhang, *ACS Appl. Mater. Interfaces*, 2020, **12**, 54884–54892.
62 B. B. Lu, W. Jiang, J. Yang, Y. Y. Liu and J. F. Ma, *ACS Appl. Mater. Interfaces*, 2017, **9**, 39441–39449.
63 S. Ameerunisha and P. S. Zacharias, *J. Chem. Soc., Perkin Trans. 2*, 1995, 1679–1682.
64 G. Agustí, S. Cobo, A. B. Gaspar, G. Molnár, N. O. Moussa, P. Á. Szilágyi, V. Pálfi, C. Vieu, M. Carmen Muñoz, J. A. Real and A. Bousseksou, *Chem. Mater.*, 2008, **20**, 6721–6732.
65 SAINT, *Program for Data Extraction and Reduction*, Bruker AXS, Inc., Madison, WI, 2001.
66 (*a*) G. M. Sheldrick, *SADABS, Program for Empirical Adsorption Correction of Area Detector Data*, University of Gottingen, Gottingen, Germany, 2003; (*b*) G. M. Sheldrick, *SHELXL-2018, Program for the Crystal Structure Solution*, University of Gottingen, Gottingen, Germany, 2018.
67 (*a*) A. L. Spek, *Acta Crystallogr., Sect. A: Found. Crystallogr.*, 1990, **46**, 194; (*b*) A. L. Spek, *J. Appl. Crystallogr.*, 2003, **36**, 7–13.
68 A. L. Spek, *Acta Crystallogr., Sect. C: Struct. Chem.*, 2015, **71**, 9–18.
69 L. Yang, D. R. Powell and R. R. Houser, *Dalton Trans.*, 2007, 955–964.
70 (*a*) V. A. Blatov, A. P. Shevchenko and V. N. Serezhkin, *J. Appl. Crystallogr.*, 2000, **33**, 1193; (*b*) V. A. Blatov, A. P. Shevchenko and D. M. Proserpio, *Cryst. Growth Des.*, 2014, **14**, 3576–3586.
71 (*a*) L. L. Gao, Q. N. Zhao, M. M. Li, L. M. Fan, X. Y. Niu and X. Q. Wang, *CrystEngComm*, 2017, **19**, 6651–6659; (*b*) S. L. Zhang, S. Gao, X. Wang, X. He, J. Zhao and D. R. Zhu, *Acta Crystallogr., Sect. B: Struct. Sci., Cryst. Eng. Mater.*, 2019, **75**, 1060–1068; (*c*) S. Geranmayeh and A. Abbasi, *J. Inorg. Organomet. Polym. Mater.*, 2013, **23**, 1138–1144; (*d*) L. Heidari, M. Ghassemzadeh, D. Fenske, O. Fuhr, F. Mohsenzadeh and V. Bon, *J. Solid State Chem.*, 2021, **296**, 122011.